INSTITUTE OF PHYSICS PUBLISHING JOURNAL OF PHYSICS G: NUCLEAR AND PARTICLE PHYSICS

J. Phys. G: Nucl. Part. Phys. **28** (2002) 649–663 PII: S0954-3899(02)33713-7

A new technique for measuring *g* factors of excited states in fission fragments using large arrays of Ge detectors

D Patel[1], A G Smith[1], G S Simpson[1,4], R M Wall[1], J F Smith[1], O J Onakanmi[1], I Ahmad[2], J P Greene[2], M P Carpenter[2], T Lauritsen[2], C J Lister[2], R F Janssens[2], F G Kondev[2], D Seweryniak[2], B J P Gall[3], O Dorveaux[3] and B Roux[3]

[1] Schuster Laboratory, The University of Manchester, Manchester, M13 9PL, UK
[2] Physics Division, Argonne National Laboratory, Argonne, Illinois, IL 60439, USA
[3] Institut de Recherches Subatomique, CNRS-IN2P3 et Université Louis Pasteur, 67037, Strasbourg, France

E-mail: dp@mags.ph.man.ac.uk

Received 13 February 2002
Published 4 March 2002
Online at stacks.iop.org/JPhysG/28/649

Abstract

The theory behind a new, three-dimensional analysis technique for the measurement of time-integral, perturbed angular correlation (IPAC) functions is presented. The new technique is described in relation to existing methods and in terms of its specific application to a large, Ge-detector array. The effective application of the new technique is demonstrated with results from an experiment where the *g* factors of excited states in ^{252}Cf, secondary fission fragments were determined. A ^{252}Cf source, sandwiched between two iron foils and placed in a saturated magnetic field at the centre of the Gammasphere detector array, was used to make IPAC measurements of prompt γ rays in order to deduce Larmor precession angles of stopped fragments in iron. The *g* factor of the $I^{\pi} = 2^{+}$ state in ^{104}Mo was thus measured to be $g = +0.248(22)$. This new measurement shows a factor-of-5 improvement to the precision which has previously been attained in more conventional experiments.

1. Introduction

The accurate measurement of excited-state *g* factors has long been of great experimental significance due to the valuable role that they play in the understanding of nuclear structure. For an arbitrary nuclear state of spin *I*, the *g* factor is defined as

$$g = \frac{\mu}{I} \tag{1.1}$$

[4] Present address: Institut Laue-Langevin, 38042, Grenoble, France.

where the magnetic moment, μ, is expressed in units of the nuclear magneton, μ_n, and the spin is expressed in units of $\hbar$. Experimental g-factor measurements serve a wide range of purposes. They often provide valuable, direct information on the purity of single-particle configurations in near-magic nuclei as well as an excellent means of assessing the extent of collectivity in rotational nuclei. In addition, neutron and proton contributions to the angular momentum can also be determined.

A wide variety of experimental techniques exist for the measurement of excited-state g factors. Most methods are accelerator-based and the relative merits and successes of such experiments are discussed in a recent review by Stuchbery [1]. Measurements involving the use of fission fragments can be found, for example, in the studies of Wolf *et al* [2] and Gill *et al* [3] where g-factor measurements were made on nuclear excited states populated from β decay following neutron-induced fission. More recently, however, a new technique, involving the spontaneous fission of ^{252}Cf as a production mechanism, was employed with the Euroball III detector array in order to determine g factors in several, $A \sim 150$, secondary fission fragments [4]. The use of a spontaneous fission source has two advantages over the β-delayed method—access to higher initial spins and access to some of the most neutron-rich nuclei available experimentally. The Euroball III study [4], herein referred to as Experiment EB97, made use of a ^{252}Cf source sandwiched between two gadolinium foils and held at a temperature of 86 K by liquid-nitrogen cooling. The precessions of fission fragments were deduced from time-integral, perturbed angular correlation (IPAC) measurements. However, the analysis of experimental data was limited to the measurement of small precession angles due to the use of a first-order approximation. Lower-than-expected hyperfine fields were also detected and this was attributed to damage of the gadolinium lattice from fission fragments.

The experiment described in this paper, herein referred to as Experiment GS00, is an extension of the original work done in Experiment EB97 [4]. For GS00, the gadolinium foils were replaced with iron foils which did not require liquid-nitrogen cooling and whose impurity hyperfine fields were known to vary less between samples. Full use was made of the entire Gammasphere array by successfully carrying out IPAC measurements in a fully three-dimensional (3D) analysis technique. The new analysis technique was found to be more appropriate for the measurement of larger precession angles than the method employed for the analysis of data from Experiment EB97 [4]. The general details of this new analysis technique are presented in section 2 and the very specific case of a direct application to the Gammasphere array is described in section 3.

In section 4, a new g-factor measurement for the 2^+ state in ^{104}Mo is presented. Recent work by Mantica *et al* [5] has enabled analysis of the systematic behaviour of 2^+-state g factors in even–even Mo isotopes beyond the $N = 50$ neutron shell closure. The complete set of results from Experiment GS00, including the previously unknown 2^+-state g factors in ^{106,108}Mo, are the subject of a forthcoming paper.

2. Theory

The measurement of nuclear magnetic dipole moments is based on the observation of the magnetic hyperfine interaction. In semi-classical terms, the presence of an extra-nuclear magnetic field causes the spin vector, $\boldsymbol{I}$, to precess about the field direction at the Larmor precession frequency, ω, given by [6]

$$\omega(t) = -g\frac{\mu_n}{\hbar}B(t) \tag{2.1}$$

where $B(t)$ is the impurity hyperfine field strength in tesla. In this study, only static-field measurements are considered. With particular reference to Experiments EB97 [4] and

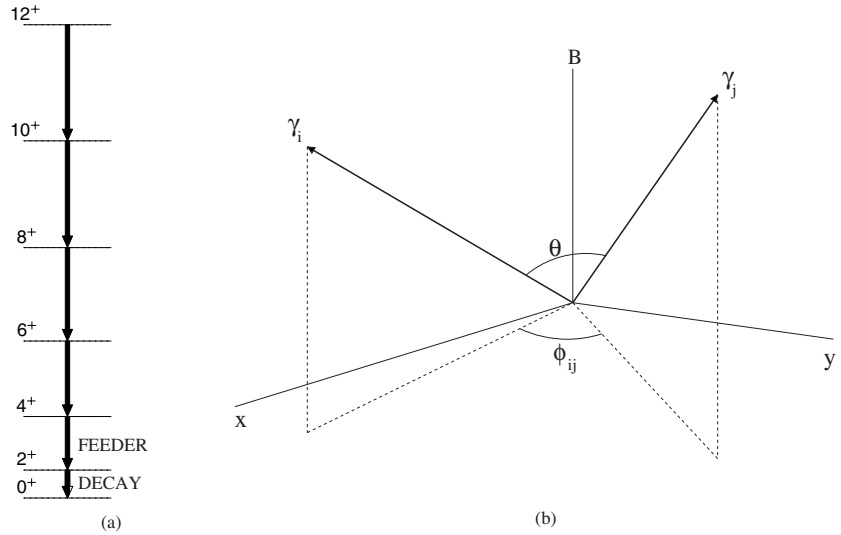

Figure 1. (a) The ground-state band of a generic even–even nucleus with the feeding and decaying γ rays for the 2^+ state shown. (b) A diagram showing the various angles described in the text. The magnetic field is chosen to be along the z-axis. Two γ rays, γ_i and γ_j, are detected at spherical polar coordinates (θ_i, ϕ_i) and (θ_j, ϕ_j), respectively. The azimuthal seperation between these two γ rays is $\phi_{ij} = \phi_j - \phi_i$ and the angle between them (in the unique plane that contains both) is θ.

GS00, the assumption that stopped fission fragments experience only static magnetic fields is reasonable—especially for low-spin states which are assumed to be populated long after the fragment has stopped within the host lattice. B and ω are, therefore, assumed to be time-independent and for a state with mean lifetime τ, equation (2.1) can be rewritten as

$$\phi_{\mathrm{p}} = -g\frac{B\mu_{\mathrm{n}}\tau}{\hbar} \tag{2.2}$$

where ϕ_{p} is the average precession angle observed during the lifetime of the state.

2.1. γ ray angular correlations and geometry

Shown in figure 1(a) is the ground-state band of an arbitrary, even–even nucleus. The 2^+ state in such a nucleus is used as an example. It can be described as being *fed* by a $4^+ \rightarrow 2^+$ γ ray from above and as *decaying* via the emission of a $2^+ \rightarrow 0^+$ γ ray. Figure 1(b) depicts a situation in which feeding and decaying γ rays, γ_i and γ_j, are detected at spherical polar coordinates (θ_i, ϕ_i) and (θ_j, ϕ_j), respectively.

For quadrupole transitions, such as those shown in figure 1(a), the anisotropy, W, in the relative direction of emission is given by the angular correlation function (ACF)

$$W(\cos\theta) = 1 + a_2 P_2(\cos\theta) + a_4 P_4(\cos\theta) \tag{2.3}$$

where θ is the angle between the γ rays as shown in figure 1(b) and P_2, P_4 are Legendre polynomials. The coefficients, a_2 and a_4, can be theoretically determined from the initial- and final-state spin configurations but in experimental terms, they must be corrected, by factors Q_2 and Q_4, respectively, in order to account for the finite solid angles of both the detectors and the source. For the specific case of stretched, quadrupole–quadrupole radiation, the theoretical values of the a_2 and a_4 parameters are +0.102 and +0.0091, respectively. For Experiment GS00, the ^{252}Cf source was taken to be a point source of γ radiation but the 7° opening angle

subtended by each detector of the Gammasphere array required Q_2 and Q_4 to be calculated. Using the approach described by Siegbahn [9], the correction factors were found to be

$$Q_2 = 0.9779 \qquad Q_4 = 0.9278 \tag{2.4}$$

where the dependence of Q_2 and Q_4 on γ ray energy was negligible. Hence, the corrected a_2 and a_4 values were

$$a_2 = +0.0997 \qquad a_4 = +0.0084. \tag{2.5}$$

The direction of the feeding γ ray, γ_i, defines the *alignment axis* which is discussed in more detail in section 2.3. The fundamental variable of interest in the evaluation of the ACF defined by equation (2.3) is the cosine of the angle between two arbitrary detection events specified by spherical polar co-ordinates (θ_i, ϕ_i) and (θ_j, ϕ_j), respectively. From a simple, geometric perspective, it is evident that this quantity, which, for later convenience, is labelled as C_{ij}, is given by

$$C_{ij} = \cos\theta = \cos\theta_i \cos\theta_j + \sin\theta_i \sin\theta_j \cos\phi_{ij} \tag{2.6}$$

where $\phi_{ij} = \phi_j - \phi_i$.

2.2. IPAC for small precession angles

With the introduction of a static magnetic field, the precession of the nucleus and its corresponding effect on the ACF can be investigated. Here, the perturbative effect of precession is considered in terms of a simple, first-order approximation. The more complete analysis is given in section 2.3.

A particularly simple situation emerges if the angular correlation is measured only in the $\theta_i = \theta_j = 90^\circ$, xy-plane (see figure 1(b)). This situation allows equation (2.6) to be greatly simplified since the angle between two detection events is then simply the azimuthal separation between the relevant detectors. Here though, the general first-order perturbation scenario is discussed where the correlation is measured between any two, general detector positions, (θ_i, ϕ_i) and (θ_j, ϕ_j).

By definition, the Larmor precession is taken to be about the z-axis as shown in figure 1(b). Hence, the expected rate of change of the ACF as a function of precession can be expressed as

$$\frac{\partial W}{\partial \phi_{ij}} \simeq \frac{\partial W}{\partial(\cos\theta)} \frac{\partial(\cos\theta)}{\partial \phi_{ij}}. \tag{2.7}$$

The substitution of equation (2.6) and some simple algebraic manipulation leads to the expression

$$\delta W \simeq -\frac{\partial W}{\partial(\cos\theta)} S_{ij} \delta\phi \tag{2.8}$$

where $S_{ij} = \sin\theta_i \sin\theta_j \sin\phi_{ij}$. δW is thus the change in γ ray intensity at (θ_j, ϕ_j) caused by a precession of the ACF through an angle $\delta\phi$ about the z-axis and equation (2.8) should be taken to be valid only for small $\delta\phi$. This simple, first-order approximation enables the 3D geometry of the problem to be dealt with using only two geometric parameters, namely $C_{ij} = \cos\theta$ and S_{ij}. The use of two geometric parameters leads to the concept of an *angle bin*, $\mathcal{B}_{ij}$. Different pairs of detectors in a large array such as Euroball or Gammasphere may possess similar angular properties and in particular, may have identical values of C_{ij} and S_{ij} and therefore be physically equivalent in terms of the observed precession effects. Hence, the data from many pairs of detectors can be said to contribute to the total data in a single angle bin, $\mathcal{B}_{ij}$, which is unique in its C_{ij} and S_{ij} values. In section 3.1, the process of creating angle bins for the Gammasphere array using three geometric parameters is described.

For feeding and decaying γ ray energies E_{F} and E_{D}, respectively, the total number of coincidence counts for an arbitrary bin, $\mathcal{B}_{ij}$, specified by unique C_{ij} and S_{ij} values is given by

$$N(C_{ij}, S_{ij}) = N_0 \varepsilon_{ij}(E_{\mathrm{F}}, E_{\mathrm{D}}) W(C_{ij}, S_{ij}) \tag{2.9}$$

where N_0 is a normalization factor dependent on the source strength and running time and $\varepsilon_{ij}(E_{\mathrm{F}}, E_{\mathrm{D}})$ is the detection efficiency for the bin, $\mathcal{B}_{ij}$, at feeding and decaying γ ray energies, E_{F} and E_{D}, respectively. The introduction of a magnetic field, whether it be positive (+) or negative (−), requires a simple modification of equation (2.9) to include a first-order term for the perturbation caused to the existing ACF, W,

$$\begin{aligned} N(C_{ij}, S_{ij}, +) &= N_0 \varepsilon_{ij}(E_{\mathrm{F}}, E_{\mathrm{D}})[W + \delta W] \\ N(C_{ij}, S_{ij}, -) &= N_0 \varepsilon_{ij}(E_{\mathrm{F}}, E_{\mathrm{D}})[W - \delta W]. \end{aligned} \tag{2.10}$$

Use of the relationship $\delta W(C_{ij}, S_{ij}, +) = \delta W(C_{ij}, -S_{ij}, -)$ allows the formation of a *double ratio*

$$\rho_{ij}(C_{ij}, S_{ij}) = \sqrt{\frac{N(C_{ij}, S_{ij}, +)}{N(C_{ij}, S_{ij}, -)} \frac{N(C_{ij}, -S_{ij}, -)}{N(C_{ij}, -S_{ij}, +)}} \tag{2.11}$$

which, after substitution of equation (2.10), can be written as

$$\rho_{ij}(C_{ij}, S_{ij}) = \frac{W + \delta W}{W - \delta W}. \tag{2.12}$$

Substitution of equation (2.8) then leads to

$$\delta\phi = -\frac{W}{S_{ij} \frac{\partial W}{\partial(\cos\theta)}} \left[\frac{\rho_{ij}(C_{ij}, S_{ij}) - 1}{\rho_{ij}(C_{ij}, S_{ij}) + 1} \right]. \tag{2.13}$$

A useful measure of perturbations (both large and small) is the experimentally determined quantity

$$\Delta_{\mathrm{W}}(\theta_i, \theta_j, \phi_{ij}) = -\frac{1}{S_{ij}} \left[\frac{\rho_{ij} - 1}{\rho_{ij} + 1} \right]. \tag{2.14}$$

Note that if there is no perturbation, the double ratio $\rho = 1$ and therefore $\Delta_{\mathrm{W}} = 0$. In the small-angle approximation, Δ_{W} is given by

$$\Delta_{\mathrm{W_{SA}}}(\cos\theta) = \frac{1}{W} \frac{\partial W}{\partial(\cos\theta)} \delta\phi. \tag{2.15}$$

The simple, linear dependence of Δ_{W} on $\delta\phi$ allows a fit of the experimentally determined Δ_{W} against the known, logarithmic derivative of $W(\cos\theta)$ in order to determine the precession angle. The obvious advantage in the use of double ratios lies in the removal of the inexactly known quantities N_0 and $\varepsilon_{ij}(E_{\mathrm{F}}, E_{\mathrm{D}})$ that are associated with experimentally determined counting rates.

The method described above was successfully employed for the analysis of data from Experiment EB97 [4] where the Euroball III array was divided into 256 bins in the space of C_{ij} versus S_{ij} in order to create 64, independent double ratios. The largest precession angle measured during the study was $\delta\phi = 0.089(17)$ rad.

2.3. The general IPAC solution

The small-angle approximation described in section 2.2 can be valid only for those cases where the precession angle is small enough to allow a simple, first-order perturbation to hold. For the more general case, the time-dependence of the ACF and the associated geometry are both considered in more detail. The *alignment axis* is still initially taken to be the direction

of the feeding γ ray, γ_i, but this precesses with time, so that the angle between the alignment axis and that of the decaying γ ray, γ_j, is given by Θ_{ij} where

$$\cos\Theta_{ij}(\theta_i, \theta_j, \phi_{ij}, t) = \cos\theta_i \cos\theta_j + \sin\theta_i \sin\theta_j \cos(\phi_{ij} - \omega t) \tag{2.16}$$

which is similar to equation (2.6) but here the time integration of the perturbed angular correlation is yet to be performed.

Substitution of equation (2.16) into the ACF of equation (2.3) and subsequent rearrangement using multiple-angle formulae, gives the time-dependent, perturbed ACF as

$$W_t(\theta_i, \theta_j, \phi_{ij}, t) = \sum_{n=0}^{n=4} f_n(\theta_i, \theta_j) \cos(n(\phi_{ij} - \omega t)) \tag{2.17}$$

where the coefficients are given by

$$\begin{aligned}
f_0 &= 1 + a_2\left(\tfrac{1}{2} + \tfrac{3}{2}A^2 + \tfrac{1}{2}B^2\right) + a_4\left(\tfrac{3}{8} + \tfrac{105}{8}A^2B^2 + \tfrac{35}{8}A^4 + \tfrac{105}{64}B^4 - \tfrac{15}{4}A^2 - \tfrac{15}{8}S^2\right)\\
f_1 &= a_2(3AB) + a_4\left(\tfrac{105}{8}B^3A + \tfrac{35}{2}A^3B - \tfrac{15}{2}AB\right)\\
f_2 &= a_2\left(\tfrac{3}{4}B^2\right) + a_4\left(\tfrac{35}{16}B^4 + \tfrac{105}{8}A^2B^2 - \tfrac{15}{8}B^2\right)\\
f_3 &= a_4\left(\tfrac{35}{8}AB^3\right)\\
f_4 &= a_4\left(\tfrac{35}{64}B^4\right).
\end{aligned} \tag{2.18}$$

The two constants, A and B, are given by $A = \cos\theta_i \cos\theta_j$ and $B = \sin\theta_i \sin\theta_j$, respectively, and the coefficients defined in equation (2.18) can be derived by substitution of the Legendre polynomials

$$P_2(\cos\theta) = \tfrac{1}{2}(3\cos^2\theta - 1) \qquad P_4(\cos\theta) = \tfrac{1}{8}(35\cos^4\theta - 30\cos^2\theta + 3) \tag{2.19}$$

into the ACF of equation (2.3). Using equation (2.17), the count rate, defined in equation (2.10), is redefined as an integral such that

$$N_{ij} = N_0\varepsilon_{ij}(E_\mathrm{F}, E_\mathrm{D})\frac{1}{\tau}\sum_{n=0}^{n=4} f_n(\theta_i, \theta_j)\int_0^\infty \mathrm{e}^{-\frac{t}{\tau}}\cos(n(\phi_{ij} - \omega t))\,\mathrm{d}t. \tag{2.20}$$

Integration over the mean lifetime of the state, τ, allows the transformation of equation (2.20) into a quantity dependent on the average precession angle, $\phi_\mathrm{p} = \omega\tau$,

$$N_{ij}(\phi_\mathrm{p}) = N_0\varepsilon_{ij}(E_\mathrm{F}, E_\mathrm{D})\sum_{n=0}^{n=4}\frac{f_n(\theta_i, \theta_j)}{\left(1 + n^2{\phi_\mathrm{p}}^2\right)}[\cos(n\phi_{ij}) + n\phi_\mathrm{p}\sin(n\phi_{ij})]. \tag{2.21}$$

This is the general equation to describe the effect of precession through a mean angle, ϕ_p, on the count rate in some arbitrary angle bin specified by three angular parameters, $(\theta_i, \theta_j, \phi_{ij})$. Unlike the two-parameter approximation of equation (2.10), it is valid for all precession angles in the full, 3D geometry. Comparison between equation (2.21) and equation (2.10) enables definition of the perturbed ACF,

$$\begin{aligned}
W_\mathrm{p}(\phi_\mathrm{p}) &= \frac{N_{ij}(\phi_\mathrm{p})}{N_0\varepsilon_{ij}(E_\mathrm{F}, E_\mathrm{D})}\\
&= \sum_{n=0}^{n=4}\frac{f_n(\theta_i, \theta_j)}{\left(1 + n^2{\phi_\mathrm{p}}^2\right)}[\cos(n\phi_{ij}) + n\phi_\mathrm{p}\sin(n\phi_{ij})].
\end{aligned} \tag{2.22}$$

Equation (2.22) can be alternatively expressed as

$$W_\mathrm{p}(\phi_\mathrm{p}) = \sum_{n=0}^{n=4}\frac{f_n(\theta_i, \theta_j)}{\left(1 + n^2{\phi_\mathrm{p}}^2\right)^{\frac{1}{2}}}\cos(n(\phi_{ij} - \Delta_\mathrm{p})) \tag{2.23}$$

where $\tan(n\Delta_{\rm p}) = n\phi_{\rm p}$. Each term in the expansion of equation (2.23) consists of a product of two factors. The first is responsible for an attenuation to the nth term in the expansion and the second is responsible for a rotation of the nth term by an angle $\Delta_{\rm p}$.

The transformation $(\phi_{\rm p}, \phi_{ij}) \rightarrow (-\phi_{\rm p}, -\phi_{ij})$ applied to either equation (2.22) or (2.23) can be seen to leave the value of $W_{\rm p}$ unchanged. This symmetry leads to redefinition of the double ratio of equation (2.11) as

$$\rho_{ij} = \sqrt{\frac{N_{ij}(\theta_i, \theta_j, \phi_{ij}, +)}{N_{ij}(\theta_i, \theta_j, \phi_{ij}, -)} \frac{N_{ij}(\theta_j, \theta_i, -\phi_{ij}, -)}{N_{ij}(\theta_j, \theta_i, -\phi_{ij}, +)}} \tag{2.24}$$

which should be interpreted as

$$\rho_{ij}(\phi_{\rm p}) = \frac{W_{\rm p}(\theta_i, \theta_j, \phi_{ij}, +\phi_{\rm p})}{W_{\rm p}(\theta_i, \theta_j, \phi_{ij}, -\phi_{\rm p})} \tag{2.25}$$

and this, along with equations (2.25) and (2.21), can allow a nonlinear, least-squares fit analysis in order to extract the precession angle, $\phi_{\rm p}$, from the experimentally determined quantity, ρ_{ij}.

In the small-angle approximation described by section 2.2, the quantity $\Delta_{\rm W}$ was defined in equation (2.14) as a measure of perturbation. In the more general case, equation (2.14) is still useful as a means of graphically demonstrating the effects of precession. An example of this is shown in figure 7(b) where the simple, linear dependence of $\Delta_{\rm W}$ on C_{ij} and $\delta\phi$, as given in equation (2.15), is compared with a more complicated dependence involving θ_i, θ_j, ϕ_{ij} and $\phi_{\rm p}$.

An example of the application of the technique described above is presented in section 4 where the results obtained from Experiment GS00 are described.

3. Experimental details

The data from Experiment GS00 were collected over a two-week run using the Gammasphere array of detectors at the Argonne National Laboratory in Chicago, Illinois, USA. The 101, Compton-suppressed, Ge detectors were placed in their usual, approximately spherically symmetric arrangement providing a total detector efficiency of $\sim$10%.

A ^{252}Cf source of 100 μCi total activity and 3 μCi fission activity was sandwiched between two, 15 mg cm^{-2} Fe foils. The Fe foils had previously been annealed at a temperature of 650 °C for 10 min. The magnetization of these foils as a function of applied field had been measured using a magnetometer and the results showed that, with an applied field of 0.1 T, the magnetic moment of the Fe foils had reached more than 98% of the calculated maximum value.

The ^{252}Cf was electroplated onto the surface of an Fe foil and a layer of indium (200 μg cm^{-2} thick) was then evaporated over the second Fe foil. The layer of indium acted as an aid to adhesion [10] between the active foil and the second Fe foil, which was rolled on top to produce a closed source in which the fission fragments stopped in iron. The Fe–Cf–Fe sandwich was placed at the centre of the Gammasphere array as shown schematically in figure 2. A pair of small, permanent magnets providing a field of 0.2 T were placed on either side of the source along a direction conventionally reserved for the beam axis into the Gammasphere array.

The direction of the applied field was reversed approximately once every 8 h during the experiment by rotating the magnet assembly through 180°. Great care was taken to ensure that the applied magnetic field was always aligned either parallel or anti-parallel to the conventional Gammasphere beamline direction. This ensured that Larmor precessions were always about

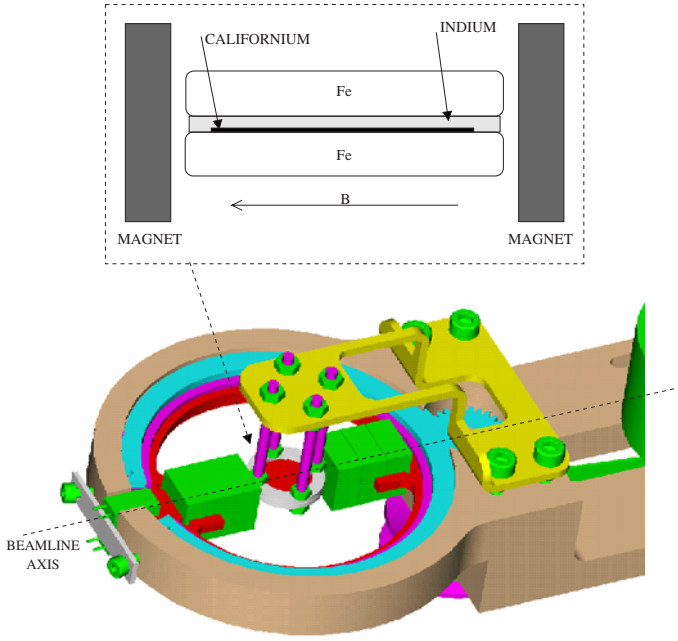

Figure 2. A schematic diagram of the apparatus used for the experiment. The rotatable magnet assembly and the fixed Fe–Cf–Fe sandwich were positioned at the centre of the Gammasphere array. The relative thicknesses of the iron, indium and californium were 15 mg cm^{-2}, 200 μg cm^{-2} and 240 ng cm^{-2}, respectively.

the beamline axis—a fact exploited in the subsequent data analysis, as described in section 2.3, which relied on the angles of detectors being defined relative to the standard beamline direction.

During the two-week run, 9.95×10^9 events (of multiplicity 3 or greater) were recorded and subsequently analysed offline. Approximately 48% of the total data were taken with the applied field pointing parallel along the beamline direction (positive-field data) with the remaining 52% taken with the applied field pointing anti-parallel to the beamline direction (negative-field data).

3.1. The division of Gammasphere into angle bins

Figure 3(a) is a plot showing the polar and azimuthal positions of each Gammasphere detector with respect to the centre of the array. The detectors are arranged in concentric rings centred about the beamline axis so that, for example, the ten detectors located at $\theta_i = 90^\circ$ make up the central ring which occupies the $z = 0$, xy-plane. There are 17 such rings in total.

To create the angular bins, all possible detector pairs were considered. As was mentioned in section 2.2, the concentric arrangement of detectors meant that many of the pairs were found to be geometrically equivalent and were therefore combined in a single angle bin $\mathcal{B}_{ij}$.

The creation of 3882 discrete angles bins was found to be representative of all $(\theta_i, \theta_j, \phi_{ij})$ combinations in the 3D geometry. A total number of 1081 independent double ratios were created in the space of $(\theta_i, \theta_j, \phi_{ij})$. The data from angle bins $(\theta_i, \theta_j, \phi_{ij})$ and $(\theta_j, \theta_i, \phi_{ij})$ were combined in the same double ratio since the constants, A and B, of equation (2.18) can be shown to be invariant under the transformation $\theta_i \leftrightarrow \theta_j$.

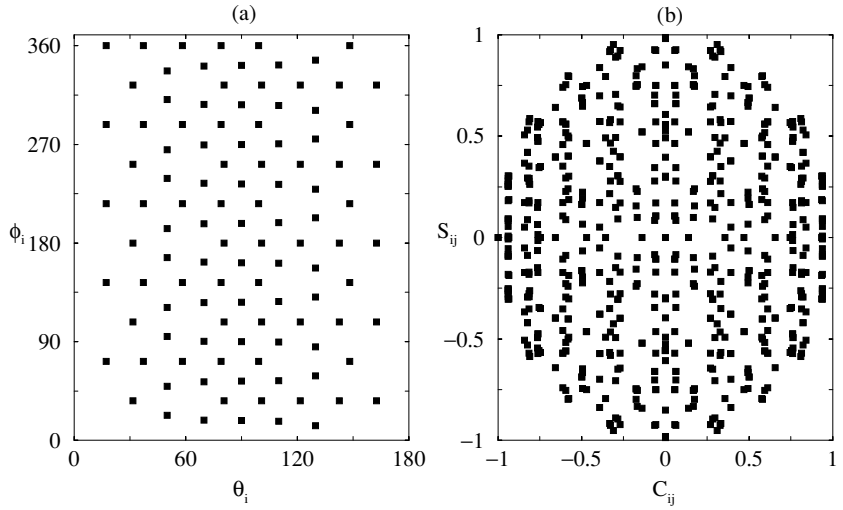

Figure 3. (a) The polar (θ_i) and azimuthal (ϕ_i) positions of the each detector within the Gammasphere array. (b) The distribution of angular bins in a space defined by the quantities C_{ij} and S_{ij}.

Figure 3(b) shows the reduction of each (θ_i, θ_j, ϕ_{ij}) angle bin into a space defined by just two geometric parameters, C_{ij} and S_{ij}, as defined in equations (2.6) and (2.8), respectively. Having ignored minor rounding errors, the 3882 bins were found to project onto 645 discrete areas in the space of C_{ij} versus S_{ij}. Further projection of the 3882 bins onto the $C_{ij} = \cos\theta$ axis allowed the graphical display of results shown in section 4. All of the bins represented in figure 3(b) occupy one of only 118 discrete positions in the linear space of C_{ij}.

3.2. Gating conditions and fragment identification

As mentioned earlier, approximately 9.95×10^9 γ ray events (of multiplicity 3 or greater) were recorded during the experiment. The appropriate data for each excited state under investigation were identified by careful selection of all events containing the required feeding and decaying γ rays.

The case of ^{104}Mo is used as an example. For IPAC measurements of the 2^+ state, the appropriate feeding and decaying γ rays are the 368 and 192 keV transitions, respectively [7]. Figure 4(a) shows the total γ ray spectrum obtained in the experiment. The ^{104}Mo transitions mentioned above are indicated. Figure 4(b) shows the spectrum produced by consecutively gating on the ^{104}Mo, 2^+ state feeding and decaying transitions in a 3D cube.

Spectra such as that shown in figure 4(b) were used as a guide in order to identify possible candidates for a new, third gate which was subsequently applied to the data set. The third gate is referred to as the *isotropic* gate, E_{I}, since the emission direction was not a factor in calculations—merely its presence in the data event. The selection of three gates, E_{F}, E_{D} and E_{I}, rather than just the two needed for an ACF measurement, served to ensure that the data under analysis were truly from the nucleus of interest and not from another, contaminant nucleus possessing similar γ ray transitions to those in the nucleus under investigation. The feeding and decaying γ rays for the 2^+ state in ^{104}Mo are a good example of such a conflict since they are identical in energy to the corresponding γ rays for the 2^+ state in ^{108}Mo. This conflict is resolved with appropriate selection of isotropic gates and the impact is lessened anyway by

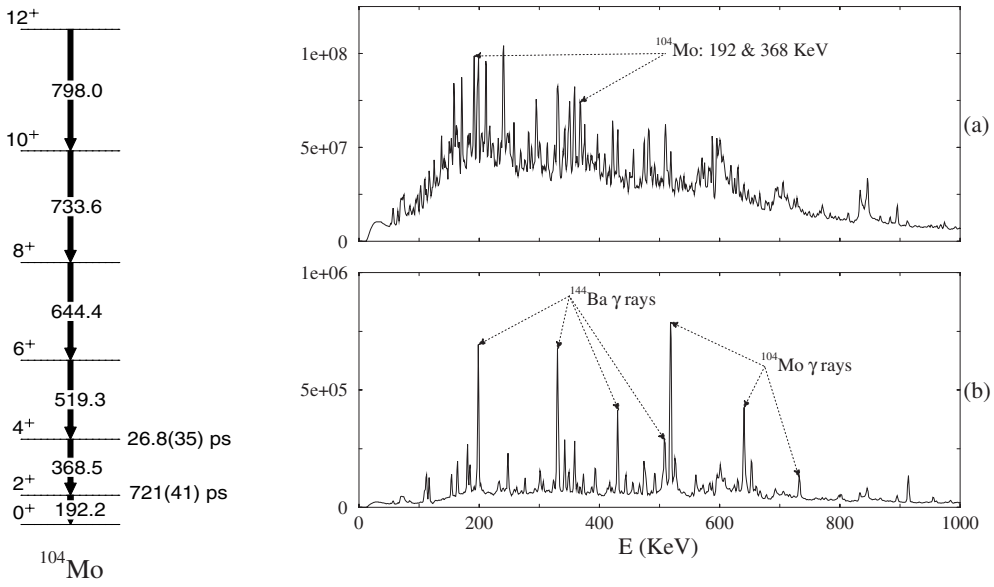

Figure 4. (a) The total γ ray spectrum obtained from Experiment GS00. Indicated are the feeding and decaying γ rays for the 2^+ state in ^{104}Mo. (b) The spectrum produced by consecutively gating on the ^{104}Mo, 2^+-state feeding and decaying γ rays. Other ^{104}Mo ground-state band γ rays are indicated. Also marked are the intense, ground-state band γ rays from ^{144}Ba—the complementary fragment produced in a 4-neutron fission event.

the fact that the ^{108}Mo production rate from ^{252}Cf fission is down by more than a factor of 4 compared to that for ^{104}Mo.

Generally, the most intense isotropic gates came from the ground-state band of the nucleus concerned. Use was also made of isotropic gates from the complementary fission fragment—the second fragment created from the binary fission of the parent, ^{252}Cf nucleus. For ^{104}Mo, the complementary fragment for a 4-neutron fission event is $^{144}_{56}\mathrm{Ba}_{88}$. The 199, 331, 432 and 509 keV ground-state transitions in ^{144}Ba [12] can clearly be identified in figure 4(b). 3-neutron fission events were also observed to occur in some cases but these were much less common.

With isotropic gates identified, a 2D matrix, $\mathcal{M}(E_\mathrm{D}, \mathcal{A})$, was produced from event-by-event data by setting appropriate E_I and E_F gates [11]. The linear axis, $\mathcal{A}$, held an arbitrary angle-bin number to represent every possible combination of $(\theta_i, \theta_j, \phi_{ij}, \pm)$ as described in section 3.1. A gate cut on the E_D-axis of $\mathcal{M}(E_\mathrm{D}, \mathcal{A})$ produced a 1D histogram which then allowed the creation of double ratios and subsequent determination of ϕ_p as described in section 2.3.

3.3. The direct measurement of the attenuation of W_p

Figure 5 shows theoretical double ratios for four different bin geometries as a function of precession angle. It is evident that for any given geometry, certain values of ρ have two different ϕ_p solutions—one solution corresponds to a relatively small precession angle and the other to a much larger precession angle.

In certain cases, the problem arose of two, statistically equivalent ϕ_p solutions being found in a nonlinear, least-squares fit. Rather than arbitrarily dismissing one solution in favour of

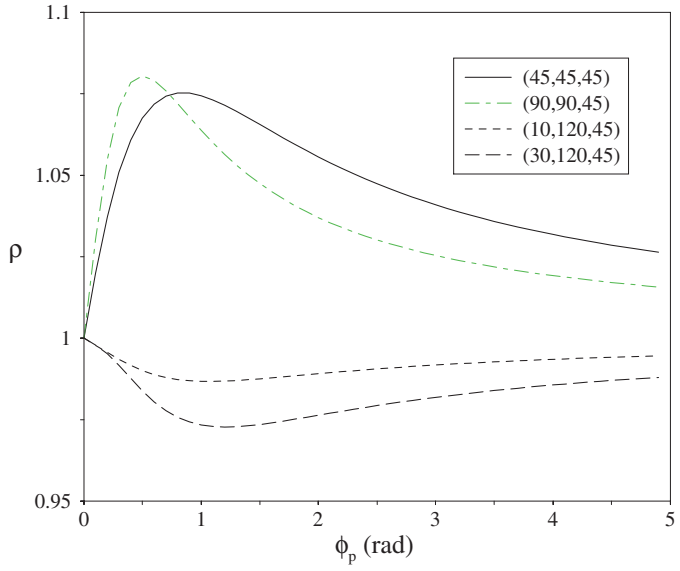

Figure 5. Four examples of double ratios and their dependence on the precession angle, ϕ_p. The numbers in brackets are the $(\theta_i, \theta_j, \phi_{ij})$ variables calculated for different bin geometries.

another, it was possible to quantitively determine the true magnitude of the precession angle (large or small) by explicitly measuring the perturbed ACF of equation (2.22).

Equations (2.22) and (2.23) showed that the ACF is subject to both rotation and attenuation as a result of Larmor precession. It was possible to combine the relevant positive- and negative-field data in such a way that the rotation term was cancelled but the attenuation term was not. Hence measurements were made of the degree of attenuation to the a_2 and a_4 parameters of the ACF. For cases where the true precession angle was large, the angular anisotropy between successive γ ray emissions was found to be strongly attenuated. Conversely, a genuinely small precession was found to have little or no effect on the anisotropy and hence the measured correlation, W_p, was found to not differ significantly from that of equation (2.3).

The positive- and negative-field data were combined to produce the attenuated ACF,

$$W_a(C_{ij}, E_F, E_D) = \frac{1}{N_0 \varepsilon_{ij}(E_F, E_D)}[N_{ij}(C_{ij}, +) + aN_{ij}(C_{ij}, -)] \tag{3.1}$$

where the normalization constant, a, was introduced in order to compensate for the difference in the amounts of positive- and negative-field data. Inspection of equation (2.22) reveals that the simple addition of positive- and negative-field data ($+\phi_p$ and $-\phi_p$, respectively) cancels the effect of the rotation of the ACF but not the attenuation. The a_2 and a_4 parameters were therefore measured by performing a linear, least-squares fit of the experimental data to equation (2.3). The measured a_2 and a_4 were then compared with the values expected for the unattenuated, $\phi_p = 0$, case as given in equation (2.5).

In order to determine W_a, the angle-bin efficiencies, $\varepsilon_{ij}(E_F, E_D)$, were measured. For an arbitrary, *individual* detector, i, the normalized counting efficiency at a photopeak energy, E_F, was taken to be

$$\varepsilon_d(E_F, i) = \frac{n_i}{\sum_{k=1}^{101} n_k} \tag{3.2}$$

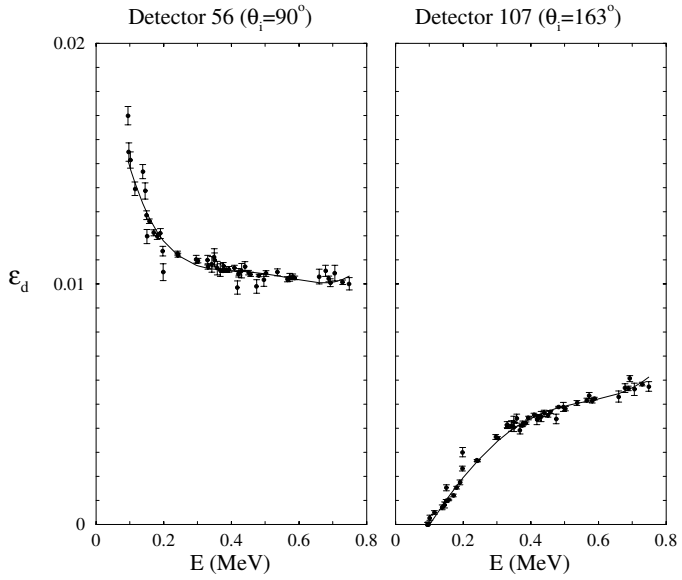

Figure 6. Normalized efficiency measurements for two different detectors. The solid lines represent fourth-order, polynomial fits to the data. The vertical axes have the same origin and scale.

where n_i is the number of counts in detector i and the sum is the total photopeak count over all 101 detectors. Hence for a *single pair* of detectors, i and j, the normalized counting efficiency for a γ ray of energy E_{F} being detected in detector i and a second γ ray of energy E_{D} being detected in detector j was taken to be

$$\varepsilon_{\mathrm{p}}(E_{\mathrm{F}}, i, E_{\mathrm{D}}, j) = \varepsilon_{\mathrm{d}}(E_{\mathrm{F}}, i)\varepsilon_{\mathrm{d}}(E_{\mathrm{D}}, j). \tag{3.3}$$

The normalized efficiency of the *angle bin* to which the detector pairing, ij, belonged was then taken to be

$$\varepsilon_{ij}(E_{\mathrm{F}}, E_{\mathrm{D}}) = \sum_{\mathrm{p}} \varepsilon_{\mathrm{p}}(E_{\mathrm{F}}, i, E_{\mathrm{D}}, j) \tag{3.4}$$

where the sum is over all *pairs* contributing to the angle bin.

The process of measuring $\varepsilon_{ij}(E_{\mathrm{F}}, E_{\mathrm{D}})$ began with the identification of intense transitions in the ground-state bands of various nuclei ranging from $^{98}_{38}\mathrm{Zr}_{60}$ through to $^{150}_{58}\mathrm{Ce}_{92}$. In order to sample the same fold distribution as used for the IPAC analysis, sets of three gates were used. Two gates, E_{I_1} and E_{I_2}, were isotropic and the third, E_ε, was the energy at which efficiency was being measured. The use of two isotropic gates meant that the angular anisotropy present in the data sample was ignored and therefore had no effect on the normalized efficiencies.

A 2D efficiency matrix, $\mathcal{M}_\varepsilon(E_\varepsilon, \mathcal{I})$, similar to that described in section 3.2, was produced from all event-by-event data by setting every combination of E_{I_1} and E_{I_2} gates possible using the ground-state band transitions of the nuclei mentioned above. The axis, $\mathcal{I}$, held the count rate in each individual detector of the array. A gate cut on the E_ε-axis of $\mathcal{M}_\varepsilon(E_\varepsilon, \mathcal{I})$ then produced a 1D histogram of the count rate in each detector at energy E_ε.

Figure 6 is a plot of the measured efficiencies of two detectors located in different positions within the Gammasphere array.

Detector 56 was located in the $\theta_i = 90$, central ring of detectors. Detector 107 was positioned in one of the two outermost rings of detectors closest to the conventional beamline.

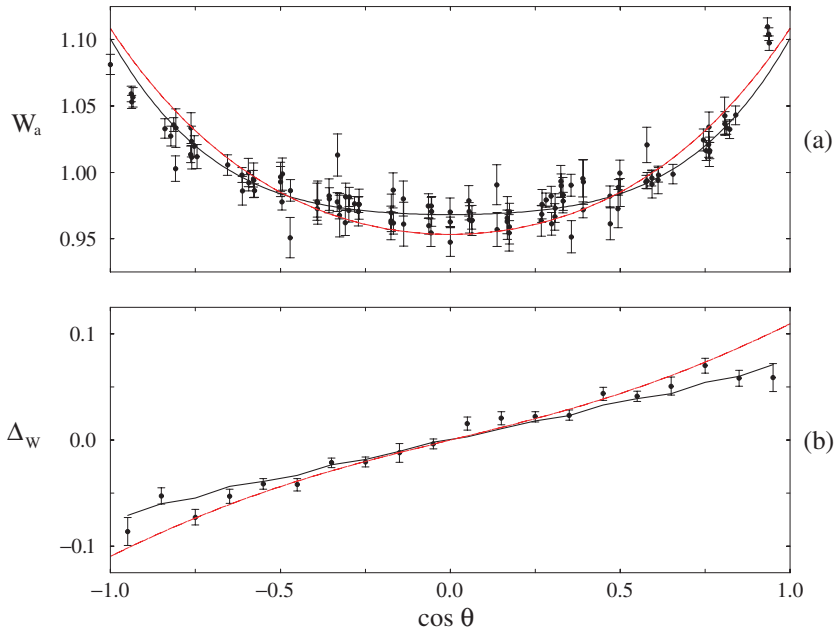

Figure 7. (a) The attenuated ACF, W_a, equation (3.1), measured for the 2^+ state in ^{104}Mo. The solid line is the fit to equation (2.22) which produced the result $\phi_p = +0.316(21)$ rad and the dashed line is the unattenuated ACF using the a_2 and a_4 parameters given in equation (2.5). (b) Δ_W, equation (2.14). The solid line represents the expected perturbation for a $\phi_p = +0.316(14)$ rad precession using the 3D analysis of section 2.3 and the dashed line is the expected perturbation using the small-angle approximation of equation (2.15). For the sake of clarity, the 118 data points in (a) have been averaged over small intervals in $\cos\theta$ to produce the 20 data points of (b).

Consequently it was found to be strongly affected by the presence of the permanent magnets shown in figure 2, especially at low γ ray energies.

Fourth-order polynomial fits, such as those shown in figure 6, were performed for all the detectors of the Gammasphere array. These were used to determine the energy-dependent counting efficiencies for each pair of detectors and then, by simple summation over relevant pair combinations, for each of the 3882 angle bins of Gammasphere.

An example of the use of efficiency curves in the direct measurement of W_a is presented in section 4.

4. Results

To demonstrate the effective application of the techniques described above, results for the 2^+ state in ^{104}Mo are presented as an example. The lifetime of the state is $\tau = 1.040(59)$ ns [8] and the g factor has previously been measured by Menzen *et al* [13] to be $g = +0.19(11)$.

Figures 7(a) and (b) are the results of the IPAC measurements for the 2^+ state in ^{104}Mo. Analysis of the double ratios, ρ_{ij}, as defined in equation (2.24), gave the precession angle as $\phi_p = +0.316(21)$ rad.

The data shown in figure 7(a) were generated using equation (3.1) and then fitted to the ACF of equation (2.3) to produce the results

$$a_2 = +0.0794(86) \qquad a_4 = +0.0212(23). \tag{4.1}$$

A useful quantity, which incorporates both the a_2 and a_4 parameters, is the *anisotropy*,

$$A = \frac{W(180^\circ)}{W(90^\circ)} - 1 = 0.1368(24) \tag{4.2}$$

which is only slightly reduced from the unattenuated anisotropy, $A = 0.1625$, as calculated using the theoretical maximum values, $a_2 = 0.0997$ and $a_4 = 0.0084$, and is, therefore, consistent with a relatively small precession angle of $\phi_p = +0.316(21)$ rad. Figure 7(b) clearly justifies the use of a more rigorous analysis technique as opposed to the small-angle approximation. The data points are better described by a full, 3D analysis rather than a simple, first-order perturbation.

Using the precession angle of $\phi_p = +0.316(21)$ rad and a hyperfine impurity field of $B = -25.6(1)$ T for Mo atoms implanted in an Fe host [14], equation (2.2) revealed the g factor to be

$$g = +0.248(22) \tag{4.3}$$

which is in good agreement with the previously measured value of $g = +0.19(11)$, as measured by Menzen *et al* [13], and which also represents a factor of 5 improvement to the precision with which the g factor has been previously measured.

5. Conclusion

This paper describes the general formalism of IPAC measurements and its application to a multi-element detector array in a proper, 3D analysis. Details have been provided on the analysis technique and its relation to existing methods. Experimental results in the form of an IPAC measurement on prompt γ rays from ^{104}Mo have been presented in order to demonstrate the effectiveness and suitability of the new method. The full experimental results will be presented in a forthcoming paper.

Acknowledgments

This project was supported by the UK EPSRC and the US Department of Energy under contract no W-31-109-ENG-38. The authors are also indebted for the use of the ^{252}Cf to the Office of Basic Energy Sciences, US Department of Energy, through the transplutonium element production facilities at the Oak Ridge National Laboratory. One of us (AGS) would like to acknowledge the receipt of an EPSRC Advanced Fellowship and a further three of us (DP, GSS, OJO) acknowledge receipt of EPSRC student grants at the time of the experiment. One of us (RMW) was supported financially by the European Commission, under the TMR network.

References

[1] Stuchbery A E 2001 *Nucl. Phys.* A **682** 470
[2] Wolf A, Berant Z, Warner D D, Gill R L, Shmid M, Chrien R E, Peaslee G, Yamamoto H, Hill J C, Wohn F K, Chung C and Walters W B 1983 *Phys. Lett.* B **123** 165
[3] Gill R L, Warner D D, Mach H, Piotrowski A, Wolf A, Hill J C, Wohn F K, Winger J A and Fogelberg B 1986 *Phys. Rev.* C **33** 1030
[4] Smith A G, Simpson G S, Billowes J, Durell J L, Dagnall P J, Freeman S J, Leddy M, Roach A A, Smith J F, Jungclaus A, Lieb K P, Teich C, Gall B J, Hoellinger F, Schulz N, Ahmad I, Green J and Algora A 1999 *Phys. Lett.* B **453** 206

[5] Mantica P F, Stuchbery A E, Groh D E, Prisciandaro J I and Robinson M P 2001 *Phys. Rev.* C **63** 034 312
[6] Cerny J (ed) 1974 *Nuclear Spectroscopy and Reactions (Part C)* (New York: Academic) 93
[7] Martin M J (ed) 1991 *Nucl. Data Sheets* **64** 24
[8] Liang M, Ohm H, De Stutter B, Sistemich K, Fazekas B and Molnar G 1991 *Z. Phys.* A **340** 223
[9] Siegbahn K (ed) 1968 *Alpha-, Beta-, and Gamma-Ray Spectroscopy (Part 2)* (Amsterdam: North-Holland) 1192
[10] Teich C, Jungclaus A and Lieb K P 1998 *Nucl. Instrum. Methods* A **418** 365
[11] Smith A G 1996 *Nucl. Instrum. Methods* A **381** 517
[12] Martin M J (ed) 1989 *Nucl. Data Sheets* **56** 635
[13] Menzen G, Wolf A, Lawin H, Lhersonneau G and Sistemich K 1985 *Z. Phys.* A **321** 593
[14] Rao G N 1985 *Hyperfine Interact.* **24** 1119